Proceedings of the 7th IFAC Symposium on Mechatronic Systems, Loughborough University, UK, September 5-8, 2016

Robust Surface Abnormality Detection for a Robotic Inspection System

Sara Sharifzadeh, Istvan Biro, Niels Lohse, Peter Kinnell

EPSRC Centre for Innovative Manufacturing in Intelligent Automation
Wolfson School of Mechanical, Electrical and Manufacturing Engineering
Loughborough University

UK, (Tel: +44 (0)1509 227146, E-mail: P.Kinnell@lboro.ac.uk)

Abstract: The detection of surface abnormalities on large complex parts represents a significant automation challenge. This is particularly true when surfaces are large (multiple square metres) but abnormalities are small (less than one mm square), and the surfaces of interest are not simple flat planes. One possible solution is to use a robot-mounted laser line scanner, which can acquire fast surface measurements from large complex geometries. The problem with this approach is that the collected data may vary in quality, and this makes it difficult to achieve accurate and reliable inspection. In this paper a strategy for abnormality detection on highly curved Aluminum surfaces, using surface data obtained by a robot-mounted laser scanner, is presented. Using the laser scanner, data is collected from surfaces containing abnormalities, in the form of surface dents or bumps, of approximately one millimeter in diameter. To examine the effect of scan conditions on abnormality detection, two different curved test surfaces are used, and in addition the lateral spacing of laser scans was also varied. These variables were considered because they influence the distribution of points, in the point cloud (PC), that represent an abnormality. The proposed analysis consists of three main steps. First, a pre-processing step consisting of a fine smoothing procedure followed by a global noise analysis is carried out. Second, an abnormality classifier is trained based on a set of predefined surface abnormalities. Third, the trained classifier is used on suspicious areas of the surface in a general unsupervised thresholding step. This step saves computational time as it avoids analyzing every surface data point. Experimental results show that, the proposed technique can successfully find all present abnormalities for both training and test sets with minor false positives and no false negatives.

Keywords: Automatic abnormality detection, Point Cloud analysis, Feature extraction, Feature classification, Adaptive smoothing, surface inspection.

1. INTRODUCTION

In many manufacturing applications, surface inspection is a critical part of the manufacturing process. For components that are large and highly sculptured, reliably searching for small surface abnormalities represents a difficult, time consuming and costly task. The complexity of the task often means this type of inspection is performed only by human experts; however, due to limitations in accuracy, consistency, speed and reliability there is a strong motivation to automate these inspection tasks. One possible solution is to use a robot-mounted laser line scanner. Laser line scanners are fast contactless sensors that can be used for the measurement and inspection of surfaces. The low weight and compact size of laser line scanners allow them to be integrated with industrial robots to form a flexible inspection system.

A significant quantity research has been conducted on the use of laser scanners for automatic inspection in manufacturing applications. One group of strategies for surface abnormality detection are based on the use of an existing ideal CAD (computer aided design) model. (Newman & Jain, 1995) proposed an automatic visual inspection system for abnormality detection using range images and computer-aided design (CAD) models. An alternative approach is presented by (Lilienblum, Albrecht, Calow, & Michaelis, 2000) about the automatic detection of small dents in car bodies by training an artificial neural network (ANN) using measurements of several master work pieces; (Hong-Seok & Mani, 2014; Prieto et al., 2000; Prieto, Redarce, Lepage, & Boulanger, 2002) are other examples of this approach. Other techniques that are independent of a CAD model include (Schall Oliver, Belyaev Alexander, 2005), where a noise removal method was proposed to detect simple deformations in a point cloud (PC) that resembles outliers in a smooth surface. However, the parameter selection for this method is not intuitive, and it is not appropriate when the deformations do not resemble outliers. In (H. Woo, E. Kang, Semyung Wang, 2002), a technique for PC segmentation based on

octree structures and recursive subdivision of the volume of a 3D mesh was introduced. The subdivision was performed based on thresholding the standard deviation of surface normal. A problem with this approach is that the threshold must be selected appropriately, to exclude the expected surface form and roughness (including measurement noise), but include the surface features that must be detected. Similarly, (Yogeswaran & Payeur, 2012) combined enhanced octree-based feature extraction with segmentation and classification. Deviation in surface normal was also used as point weights in (Pauly, Keiser, & Gross, 2003). At different scales, different local neighbourhood sizes were used to compute point weights, and the corresponding weights to strong persistent surface features exceeded a threshold across multiple scales. This method is appropriate if the structure of the features allows quantification based on scale-dependant variation and the choice of an appropriate threshold is not an issue.

In this paper, the problem of abnormality detection, when using a robot mounted 2D laser scanner is considered. This application provides challenging PCs that contain variable noise and scan resolution due to object surface curvature and the relative position of the scanner from the object. To investigate this problem, two common scenarios are considered; high resolution and high line space variability (H-H) and low resolution but low line space variability (L-L). The scan line spacing in the PC of the two cases is firstly different due to the robot controlled scan steps, but also, the object curvature and the robot position causes geometrically dependent changes in line spacing. Due to these issues, the measured set of points that represents a given surface abnormality is not always consistent. In this paper a robust defect detection strategy, that is able to cope with inconsistent point spacing, is presented. The proposed method consists of a pre-processing step, a feature extraction and training step and finally a test step. The main contribution of this work is addressing the variable quality of data collected within a single PC. This is done by detecting and excluding the local regions of the PC with excessively high levels of noise, but noting the locations for follow-up scans or inspections. Then, where possible, adaptive filtering of local patches before feature extraction is used to reduce the number of false positives from lower quality data. Once suitable data is identified a defined set of structural and statistical features capable to deal with typical line spacing variations are proposed.

The paper is organized as follows; Section 2 describes the equipment setup used for this work. Section 3 is about PC analysis techniques. The experimental results are presented in section 4 and finally there is a discussion and conclusion in sections 5 and 6 respectively.

2. DATA AQUISITION

2.1 Laser Scanner

A custom made laser scanner consisting of a Flexpoint MVnano, 450nm, 1mW, 30° fan angle, focusable laser and a Basler acA1600-20gm GigE camera was used. Choosing a triangulation angle of 35° and a stand-off distance of 110mm, the scanner resolution is calculated to be 84µm/pixel (X direction, along the laser line) and 146µm/pixel (Z direction, depth – this can be substantially improved by fitting across the imaged laser line width, achieving sub-pixel resolution, as done by Halcon at the time of PC extraction – see Data sets in section 2.2). This laser scanner was mounted on a Fanuc LR Mate 200 iC industrial robot arm, driven by a R-30/A Mate controller (Fig. 1). Moving the scanner with the robot arm over an object allowed us to scan the object, with a resolution in Y direction defined only by the robot motion. The robot path was chosen such that the laser scanner should always be normal and at the same stand-off distance to the currently investigated part of the target object. This allowed us to scan large objects, having substantial curvature and height variation, without losing laser scanner data due to exceeding the working distance (field of depth) of the scanner or due to signal loss occurring at high angles (attributed to light scattering and back-reflection). However, this path was generated from the assumed (estimated) target geometry, obtained either via few sample points (interpolated) or via estimated surface modelling (mathematical function). As a consequence, the scanning path may not always accurately follow the object surface, resulting in sub-optimal data quality, especially for highly irregular surfaces. Additionally, the scan was performed with fixed step size in the Y direction (dY), resulting in potentially varying scan line spacing L_i on a curved object (see Fig.2, constant dY, varying L_i).

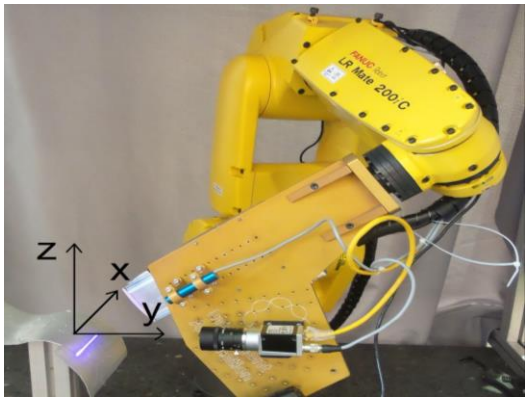

Fig. 1. The laser scanner setup mounted on a robot arm

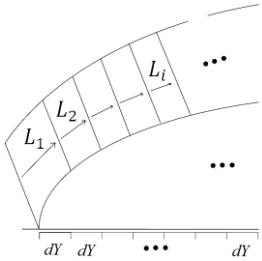

Fig. 2. The inconsistent line spacing due to robot path following.

2.2 Data Sets

Two pieces of aluminium were used for test surfaces; one was formed into a curved shape and was scanned with lower resolution resulting from a robot step size of 0.5 mm (L-L), and the second has slightly higher curvature and was scanned

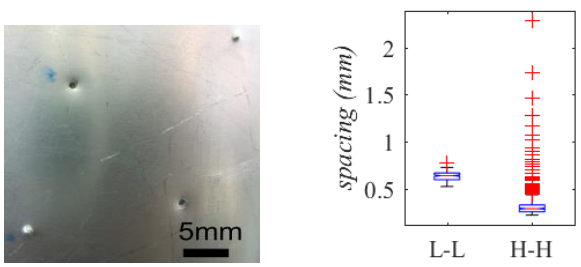

Fig. 3. (a) The local abnormalities on the Aluminium object. (b) Boxplots of the line spaces for the two PCs. The central mark is the median, the edges of the box are the 25th and 75th percentiles, the whiskers extend to the most extreme data points and the red crosses are outliers.

in higher resolution with a robot step size of 0.25 mm (H-H). Both objects contain distinct features, such as dents and bumps of about millimetre in diameter as shown in (Fig. 3-a). In both cases, identical laser scanner settings were used. Subsequent laser scanner point cloud extraction and object reconstruction was performed using the Halcon image processing software library. As each laser scanner image was taken, it was transformed into a common coordinate system, based on robot position to create a full PC representing the scanned object. Examples of the two PCs can be seen in (Fig. 4). As can be seen, the line spacing is not constant in both PCs due to the reasons explained in the previous section. The line spacing variability L_i is shown as boxplots of the adjacent lines spaces in (Fig. 3-b). In addition, a ratio is computed as ($r = \frac{\max(L_i)}{\min(L_i)}$) for each data set so that, $r_{L-L} \approx 1.488$ and $r_{H-H} \approx 10.31$, that also indicates the level of spacing variation in each case. Comparing the line spaces to the abnormality sizes in (Fig. 3-a) shows that an abnormality can be seen at least in two or three lines in most parts of the PCs. However, they might be missed if they are located around the few number of outlying lines with more than one millimetre spacing.

When using a 2D laser scanner, it is common to have variation in the quality of PC. This is due to the condition of the scanned surface, and also the orientation and position of the laser scanner relative to the surface (see section 2.1). As a result, care must be taken in the choice of the threshold value used for laser line segmentation from the image profiles. The typical threshold value that acts as cut-off point for line segmentation is high (e.g. 100) so that, points that do not pass this threshold are not segmented. Based on Halcon documentation (MVTec Software GmbH, München, 2015), the position of a scanned line profile in an image is determined column by column with sub-pixel accuracy by computing the centre of gravity of the grey levels of all pixels fulfilling the condition: $g_i \geq threshold\_cutoff$. A high value of cut-off might not be appropriate for all possible measurement cases; as such in some circumstances useful data may be incorrectly discarded. A low value, on the other hand can safely keep all the line points. The drawback is that this results in noisier PC, especially in some local region. Therefore, noise removal strategies should be employed to reduce the effect of noise. In this work, low threshold values are used and noise detection and smoothing strategies are employed to alleviate the problem.

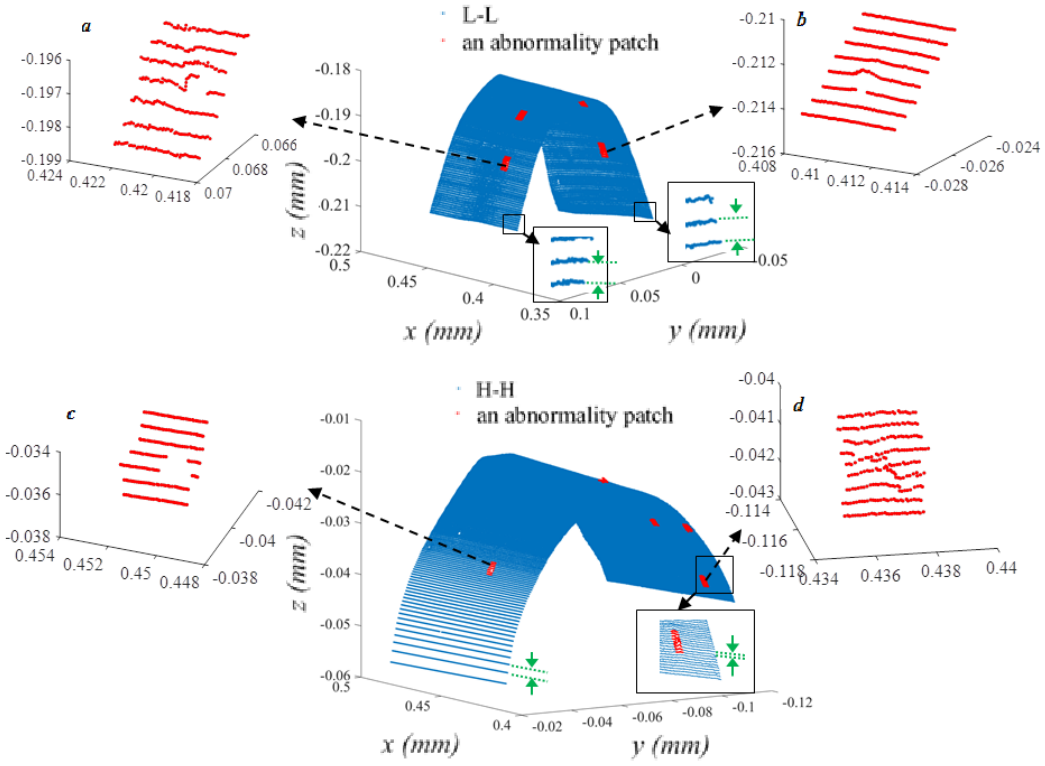

Fig. 4. 3D Plots of the two PCs and the sample abnormal regions. The line spacing is not constant.

3. PC ANALYSIS

In this section, the procedures for analysis of the PCs are explained step by step.

3.1 Pre-Processing

At this step, first a fine smoothing is performed to remove the few undesired points around the PCs. MATLAB PC noise removal function, '*pcdenoise'*, with a small neighbour size (less than five) and fine threshold value was used for this aim. While this alleviates small fluctuations over the PCs, some weak signal features in the areas of PC with high line spacing are lost after this step, as shown in (Fig. 5). In the data sets used in this work, this effect has been observed in some left side areas of H-H. One of such abnormalities is shown in (Fig. 4-c). Due to this effect, the abnormality detection model should be developed based on features that are capable of finding such cases.

Another issue is that, this fine smoothing step does not remove the significant noise in the PCs. As explained in the previous section, due to the low threshold level, noisy PCs have been formed. Basically, two different noise effects can be observed in the data sets; there is a general noise in all PC areas and even with fine smoothing it is still available. Besides that, a spread of high level of noise exists in some limited regions of PCs. To illustrate the variability in PC quality, an example set of PC data, containing such spread of noise and also a real defect, is shown in (Fig. 7). Such noisy regions can easily be misclassified as a real abnormality which increases the false positives. In this work, an adaptive local mean filter is used on small patches of PC before feature extraction to handle the first noise effect (see section 3.2) and a novel approach is taken to address the second noise spread problem, whereby all data is accepted regardless of the perceived quality. An algorithm is then applied to assess the quality of the data. In order to detect the regions with a high spread of noise, the following steps were performed.

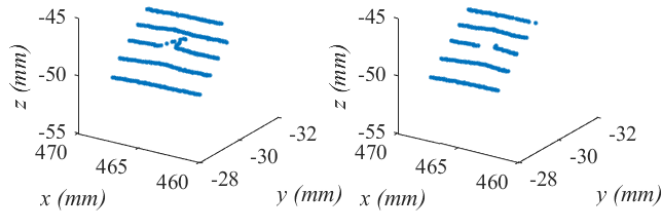

Fig. 5. The effect of fine smoothing on the weak features in high spaced scan lines (a) an abnormality before smoothing (b) after smoothing.

1. First, the most suspicious lines in terms of noise are found using the gradient function as a means of variation detection. The sum of the absolute values of point's gradients at each scanned line $l = 1,2,\dots,K$ was considered $g_l = \sum_{i=1}^{n_l} \left|\frac{\partial z_i}{\partial i}\right|$. n_l is the number of points at line l and $\frac{\partial z_i}{\partial i}$ shows the gradient of changes in Z direction at point i which is the direction that the noisy height variation occurs. Then, those $g_l s$ higher than one standard deviation from the mean were considered $g_l \geq \mu(g_l) + \sigma(g_l)$ as a list of suspicious lines. This is in fact, a comparison of all the scanned lines (between-line comparison).

2. At this step, analysis of changes is performed within selected lines at previous step. The aim is to find whether the high value of gradients in a line is due to the existence of a **local** abnormality or any other undesirable effect, in a few numbers of points in the line, or there exist a **spread** of higher number of significantly noisy points. For this aim, the selected lines are segmented into bins of fixed length (20 points), $b = 1,2,\dots,B$ and the variation in each bin is compared to the average variation of the line population. Based on our observations, a pre-assumption is that the number of regular points in a line is not less than the highly noisy ones. This means that the average variation of total bins, is closer to the regular points population rather the noisy ones. Based on this, the average sum of the absolute values of gradients at each bin μ_b as well as the total average over all the bins μ_{tb} is calculated. Then, the bins distances from the overall average (of gradients) $d_b = |\mu_{tb} - \mu_b|, b = 1,\dots,B$ is computed. Considering the distribution of distances is normal, a threshold can be defined using their average and standard deviations $\mu_d + \sigma_d$ to detect the number of irregularities in the line that exceeds the threshold. If there are few numbers of bins (e.g. less than 5) far from the average distances, there exist a local region rather than a spread noise (see Fig. 6). Such lines are excluded from the original list of suspicious lines found in the first step.

3. At this step, the suspicious lines are checked to be adjacent and those individual lines far from the other groups are excluded. A margin (e.g. 2) is also considered to include the neighbour lines before/after the group of lines in the list.

4. In the last step, the noisy points of the group of lines are found based on thresholding the $g_l s$ as performed in the first step. The detected points at each line are integrated to remove the discontinuities and the neighbour points within a margin before and after the area are also included. Furthermore, the spread of indices between the

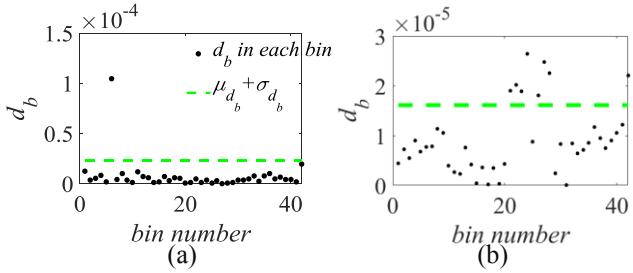

Fig. 6. The plot of d_b in a line with one abnormality (a) and a line with a noise spread area (b)

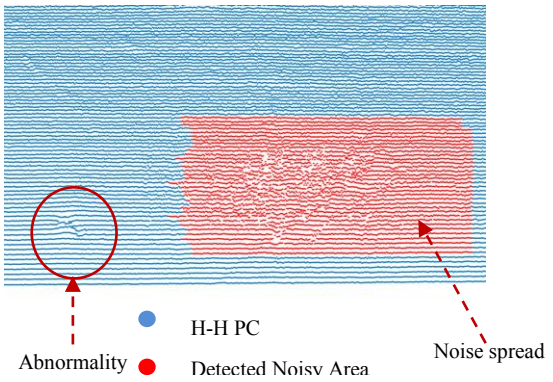

Fig. 7. A detected highly noisy region L, which is excluded from the analysis.

group of lines are equalized so that, an integrated rectangular shape area is formed as shown in (Fig. 7) and the corresponding indices are recorded in a filtered list L.

3.2 Feature Extraction

The features are defined based on the structures and characteristics of abnormalities that make them different from the regular lines. PC abnormalities are not all in similar shape. For example, the abnormalities shown in (Fig. 4-a,b) of L-L are more similar in structure to the one shown in (Fig.4-d) in H-H. However, there are abnormalities such as (Fig. 4-c), which are different in structure due to the smoothing at pre-processing step explained in section 3.1. The abnormalities similar to (a,b,d) might be confused with some noisy regions of the PCs, but the shape of those similar to (c) is different due to the missing points. The regions with a spread of high level of noise are already detected and excluded in the previous pre-processing step which alleviates the first problem. The choice of features can also help to reduce these problems.

For feature extraction, some points from different regular regions of each PC as well as some abnormal points are extracted and labelled for training. Then, a local rectangle patch of points in few millimetres is considered around each point. An adaptive local mean filter is applied to the patch for de-noising in the next step. The window size of the filter changes adaptively based on the sum of absolute values of gradients inside a patch, which shows the level of variability and noise in that patch. Thereafter, some features are extracted.

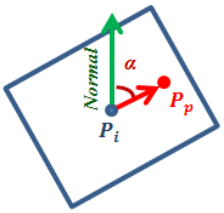

Fig. 8. Illustration of the normal to a patch and deviation angle α for a patch point P_p.

3.2.1 Normal Features

One type of classic feature for abnormality detection is surface normal. For finding the normal to a patch, a surface is fitted to the patch points and then, the normal to the fitted surface is computed (see Fig. 8). This normal is initiated from the average coordinate of all points in the patch (P_i in Fig. 8). Then, the angle between the normal and the connecting vector between P_i and each point in the patch P_p is considered (α in Fig. 8). The deviation of α from 90° increases mainly when there are variations in a patch due to the existence of an abnormality or high level of noise. Recalling that the major noisy regions are excluded at the pre-processing step and the adaptive filtering alleviates the noise, we observed that the number of points with high level of deviations (e.g. more than 50°) is more in an abnormal patch than a noisy or regular one. Therefore, the first normal feature is defined as the number of points in the patch with high degrees of deviations $f_{N1} = N(\Delta_{\alpha_p} > 50^\circ)$ so that, $\Delta_{\alpha_p} = |\alpha_p - 90^\circ|$. The second feature is defined based on the absolute value of difference between Δ_{α_p} and their population mean $\mu(\Delta_{\alpha_p})$ so that, $f_{N2} = |\Delta_{\alpha_p} - \mu(\Delta_{\alpha_p})|$. The population mean is computed using all the samples in a patch. This feature can be discriminative in conditions that the number of abnormal points with large deviations is less compared to the majority of regular points in a patch.

3.2.2 Height Features

A significant characteristic of most abnormal patches is the change in height of some points compared to the regular points. This can be quantified as a feature for each point in the patch f_{Zp}, by fitting a surface to a patch and finding the differences in the original height of the points and the corresponding height in the fitted plane.

In addition, the height changes can be considered at each line within the patch. In this case, the absolute value of height deviations from the population mean at each line is considered $f_{Zl} = |Zl_i - \mu(Zl)|$.

3.2.3 Chi-Squared statistics (χ^2)

Since in many cases, the abnormal points in a patch line have similar behaviour to a Gaussian distribution, the goodness of fit to a Gaussian is considered as a feature f_{χ^2}. The chi-squared statistic is a measure of the goodness-of-fit of the data to the Gaussian model. This statistic shows how many standard deviations each data point lies from the model:

$$\chi^2 = \sum_{i=1}^{L_p} \left(\frac{dl_i - \mu(dl)}{\sigma(dl)}\right)^2 \qquad (1)$$

Where, L_p is the number of points in a patch line, $dl_i = \sqrt{xl_i^2 + yl_i^2 + zl_i^2}$ is the Euclidean distance of each point in the line from the origin, $\mu(dl)$ and $\sigma(dl)$ are the average and standard deviations of dl_is respectively. The lower χ^2 values show better fit to a Gaussian.

3.2.4 Proximity Features

As shown in (Fig. 4-c), there are abnormalities that there is not any significant local variations in their height due to missing points. For these types of abnormalities, a proximity feature f_{prox} is defined based on maximum distance of each point in a patch from its nearest point in the adjacent lines, $f_{prox} = \max(d_{ne}, d_{pr})$ so that, d_{ne}, d_{pr} are the distances to the nearest points in the next and previous lines respectively. This feature is discriminative for the abnormality points before or after a line with a gap in, or the points located in peaks or valleys around the abnormality area. However, they might not be significantly different for the points within the line that the gap is located.

3.3 Feature Transformation

In order to increase the discrimination power of the training features (F_{tr}), the Rayleigh Quotient strategy for feature transformation is employed (Parlett, 1998). The basic idea is to transfer the features into a new space so that, the distance between the features in each class be minimized (within-class distance) while their distance to the other classes be maximized (between-class distance).

$$\arg\max_w \left(\frac{w^T S_B w}{w^T S_w w}\right) \qquad (2)$$

where, $S_B = (\mu_1 - \mu_2)(\mu_1 - \mu_2)^T$ so that, μ_1 and μ_2 are the mean of the features at each class and $S_w = (\Sigma_1 + \Sigma_2)$ so that, $\Sigma_1$and Σ_2 are the two classes covariance matrices. The solution is based on a generalized Eigen value decomposition to find the Eigen vectors W. Once this Eigen vector matrix is learnt, it can be used for transforming the training or test features (F_{tr}, F_{ts}), using its first two or three important components, $T = FW_{(1,2,3)}$. Each component is a linear combination of all the original features.

3.4 Training a Classification Model

In order to classify the transformed features T, an SVM classifier is trained. SVM is a kernel-based classification method. It is characterized based on a maximum margin algorithm. The basic idea is to map features into a high dimensional feature space using the kernel functions strategies. The classification is performed based on a linear model in this feature space whose coefficients are found based on an optimization strategy to obtain the minimum error. More information in this case can be found in chapter 12 of (Hastie, T. , Tibshirani, R. , Friedman, J. 2009).

The reason for the choice of this classification method is that it is appropriate for data sets with linear or non-linear behaviour. This is due to the use of a suitable kernel that can be found based on a model selection strategy. In this work, the LibSVM (Chang & Lin, 2011) toolbox for MATLAB is used and the choice of kernel and all the related parameters are done using an 8-fold cross validation (CV).

3.5 Test Step

A PC includes more than hundred thousands of points and applying the feature selection and classification on all of the points is highly time-consuming. In order to reduce the computational load, a fast unsupervised thresholding is applied on each PC, to find all the suspicious points including abnormalities, noisy and missing point areas. Then, all the analysis steps, including patching, adaptive filtering, feature selection and transformation and finally classification are performed only on the limited set of suspicious points. In the following this unsupervised thresholding step is described.

The common characteristic of any type of irregularity in a PC, including the highly noisy areas and abnormalities is a gap or irregular distance between some nearby points. This can be observed in (Fig. 4-(a-d) and Fig. 7). Based on this, the Euclidean distance between consecutive points at each line is computed. The irregularities are found by thresholding these distances. The threshold value is chosen empirically based on the minimum distance that might indicate an issue.

Later during the feature extraction, when a patch is defined for one of the detected points, the analysis is also performed for any other detected points in that patch. In other words, more than one detected point might share the same patch.

4. EXPERIMENTAL RESULTS

In this section the results of pre-processing, training and test steps are presented.

4.1 Pre-Processing Results

At the pre-processing step, the noise detection algorithm, has found the regions of the PCs where a high level of noise exist. (Fig. 9-a) shows the distribution of noise over the L-L PC and (Fig. 9-b)) illustrates the corresponding filtered noisy areas by the algorithm. Only the areas where the noise is widely spread are considered and the local noisy areas are left as explained in section 3.1. Similarly, the noise spread area was found for H-H.

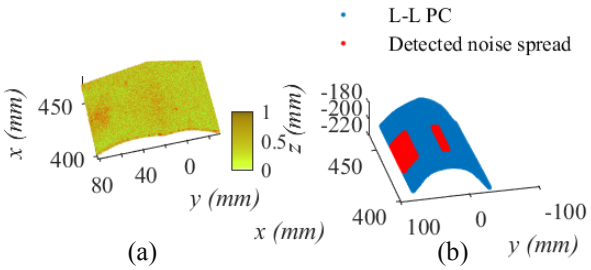

Fig. 9. (a) 3D representation of the L-L PC coloured based on the distribution of noise. (b) The corresponding filtered regions, where a spread of high level of noise exists.

4.2 Training Step Results

Based on the characteristics of the abnormalities of L-L PC, that is explained in section 3.2, five features including $f_{N1}, f_{N2}, f_{Zp}, f_{Zl}, f_{\chi^2}$ were used for training a classifier for this PC. These features are appropriate for abnormalities that have deviations from surface normal and height in their structure and can be described as a Gaussian distribution.

In the case of H-H PC, besides these five features, the maximum distance between the nearest points in the adjacent lines f_{prox} was also used. (Fig. 10) shows the features for the two classes of H-H. As can be seen, f_{N1} shows that many abnormality features have high values of ($\Delta_{\alpha_p} > 50^{\circ}$) compared to the regular ones. Those abnormality features that their deviation from the fitted surface normal (α_p) is close to 90° are close to the regular features population. That can be also be observed in f_{N2}. As expected, f_{χ^2} is lower for most of the abnormality features that have a Gaussian shape behaviour compared to the regular features. In the case of height features, f_{Zp} shows better discrimination rather than f_{Zl}. This might be due to the contribution of more number of local points to a patch height features compared to a line one. The last feature, f_{prox} shows also a discriminative effect between the two classes. This feature is very low for some of the regular PC points from the part of the H-H with low spacing and the points at the high spaced area have high values. On the other hand, most of the abnormalities are in the middle part except those located on the high spaced part of the PC which have high values. Similar behaviour was seen for the similar features of L-L.

After feature extraction, the features are transformed into a new space, using the Rayleigh Quotient for increasing the discrimination, as explained in section 3.3. The first three feature components in the new space are shown for L-L and H-H in (Fig. 11). As can be seen, the training features are well separated in the new space and the classification performance was 98.913% and 100% for the training labelled data of L-L and H-H PCs respectively.

4.3 Test Step Results

At the test step, the unsupervised thresholding was applied first to detect the suspicious points as shown in (Fig. 12-(a,c)) for L-L and H-H PCs respectively. The suspicious points that were among the initially detected highly noisy areas (from

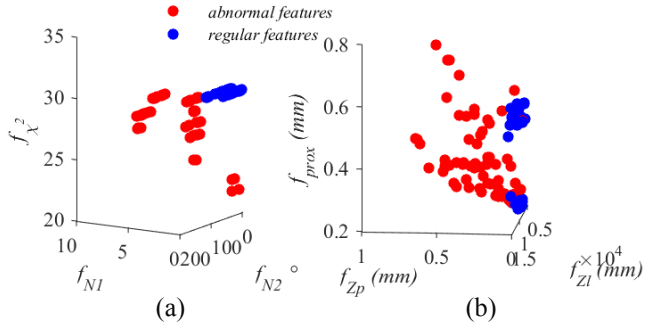

(a) (b)

Fig. 10. (a) 3D representation of f_{N1}, f_{N2} and f_{χ^2} (b) 3D representation of f_{Zp}, f_{Zl}, f_{prox} for the two training classes of H-H.

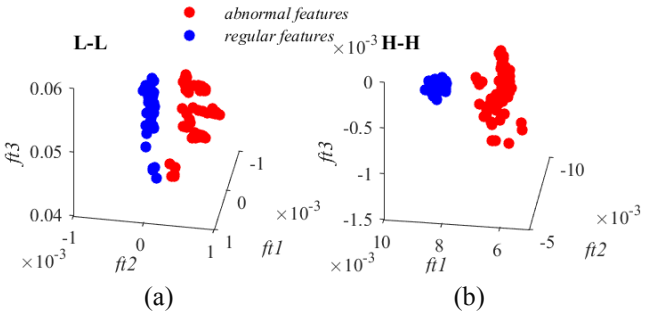

(a) (b)

Fig. 11. 3D representation of the first three components of the transformed features into a new space for L-L (a) H-H (b).

the filtered list) are shown in black colour in the images. Those points weren't considered in the next analysis steps. Then, based on the steps explained in section 3.5, the final abnormalities were classified (Fig. 12-(b,d)). The program has found all the abnormalities successfully for both PCs and there were no false positives in the case of L-L and only one false positive for H-H.

5. DISCUSSION

The obtained results show that the proposed feature extraction and transformations as well as the classification strategy can successfully find different types of abnormalities. One of the main issues in this work is the choice of features. Generally, it is desirable to choose the most discriminative features with minimum correlation or dependency. In order to test the benefit of keeping the selected features, the model performance was evaluated in terms of false positives and negatives as well as the percentage of classification performance at training step for different selections of features. Therefore, the classification model was trained separately using the two normal features, the two height features, the chi-squared and finally the proximity feature and the performance was evaluated. For both PCs the best result was obtained using all the six features. This demonstrates that each of the defined features characterize a unique aspect of the abnormalities that is important for discrimination.

6. CONCLUSION

In this paper, an abnormality detection strategy is proposed for identifying dents and bumps on curved Aluminium objects using their PC data, which is obtained by a laser scanner. The highly noisy regions of PCs are filtered at a primary step. Two different scenarios of high resolution and high spacing variability (H-H) and low resolution and low spacing variability (L-L) are studied. Six different types of features were defined and a classification model was trained. A primary unsupervised thresholding is proposed to find the most challenging points of the PC and apply the model on a limited number of points for reducing the computation load.

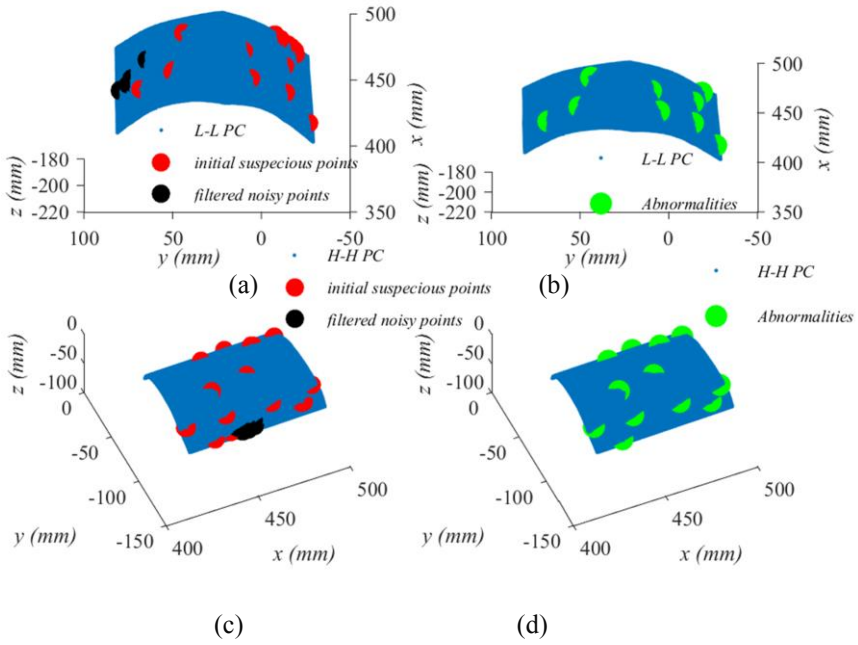

Fig. 12. (a, c) 3D representation of the initial detected points by unsupervised thresholding for L-L and H-H PCs respectively. Among these points, the highly noisy ones that were in the filtered list (L) are illustrated in black colour. (b, d) The corresponding detected abnormalities by feature extraction and classification.

REFERENCES

Blais, F. (2004). Review of 20 years of range sensor development. *Journal of Electronic Imaging*, *13*(1), 231-240.

Blais F. , Taylor J. , Cournoyer L. , Picard M. , Borgeat L. , Godin G. , Beraldin J. A., R. M. (2007). Ultra High-Resolution 3D Laser Color Imaging of Paintings : the Ultra High-Resolution 3D Laser Color Imaging of Paintings : The Mona Lisa by Leonardo Da Vinci. In *Proceedings of the 7th International Conference on Lasers in the Conservation of Artworks*. Madrid, Spain.

Chang, C., & Lin, C. (2011). LIBSVM : A Library for Support Vector Machines. *ACM Transactions on Intelligent Systems and Technology (TIST)*, *2*, 1–39.

Döring C. , Eichhorn A., Girimonte D., K. R. (2004). Improving Surface Defect Detection for Quality Assessment of Car Body Panels. *Mathware & Soft Computing*, *11*, 163–177.

H. Woo, E. Kang, Semyung Wang, K. H. L. (2002). A new segmentation method for point cloud data. *International Journal of Machine Tools & Manufacture*, *42*, 167–178.

Hastie, T. , Tibshirani, R. , Friedman, J. (2009). *The Elements of Statistical Learning*. *springer*.

Hong-Seok, P., & Mani, T. U. (2014). Development of an inspection system for defect detection in pressed parts using laser scanned data. *Procedia Engineering*, *69*, 931–936.

Lilienblum, T., Albrecht, P., Calow, R., & Michaelis, B. (2000). Dent Detection in Car Bodies. In *Pattern Recognition, 2000. Proceedings. 15th International Conference on*, 775 – 778.

MVTec Software GmbH, München, G. (2015). Reference Manual. Retrieved from http://www.halcon.com/download/documentation/

Newman, T., & Jain, A. (1995). A system for 3D CAD-based inspection using range images. *Pattern Recognition*, *28*(10), 1555–1574.

Parlett, B. N. (1998). The Symmetric Eigenvalue Problem (Society for Industrial and Applied Mathematics).

Pauly, M., Keiser, R., & Gross, M. (2003). Multi-scale Feature Extraction on Point-Sampled Surfaces. *Computer Graphics Forum*, *22*(3), 281–289.

Prieto, F., Lepage, R., Boulanger, P., Redarce, T., Industrielle, A., Villeurbanne, E., … Montr, N. O. (2000). Inspection of 3D parts using high accuracy range data. In *Proceedings of the SPIE, Volume 3966*, 82–93.

Prieto, F., Redarce, T., Lepage, R., & Boulanger, P. (2002). An Automated Inspection System. *The International Journal of Advanced Manufacturing Technology*, *19*(12), 917–925.

Schall Oliver ,Belyaev Alexander, S. H.-P. (2005). Robust Filtering of Noisy Scattered Point Data. In *Eurographics Symposium on Point-Based Graphics*.

Sequeira V., Gonçalves J. G.M., R. M. I. (1995). 3D environment modelling using laser range sensing. *Robotics and Autonomous Systems*, *16*(1), 81–91.

Yogeswaran, A., & Payeur, P. (2012). 3D Surface Analysis for Automated Detection of Deformations on Automotive Body Panels. In I. InTech (Ed.), *New Advances in Vehicular Technology and Automotive Engineering*, 978–953.